Ultrasonics 94 (2019) 117–123

Contents lists available at ScienceDirect

Ultrasonics

journal homepage: www.elsevier.com/locate/ultras

Short communication

Four-dimensional optoacoustic monitoring of tissue heating with medium intensity focused ultrasound

Francisco Javier Oyaga Landa[a,b,1], Silvia Ronda Penacoba[c,1], Francisco Montero de Espinosa[c], Daniel Razansky[a,b], Xosé Luís Deán-Ben[a,*]

[a] Institute for Biological and Medical Imaging (IBMI), Helmholtz Center Munich, Neuherberg, Germany
[b] School of Medicine, Technical University of Munich, Germany
[c] ITEFI-CSIC, Institute of Physics and Communication Technologies, Madrid, Spain

ARTICLE INFO

Keywords:
Thermal treatment monitoring
Optoacoustic tomography
Photoacoustic imaging
Temperature monitoring
Therapeutic ultrasound

ABSTRACT

Medium-intensity focused ultrasound (MIFU) concerns therapeutic ultrasound interventions aimed at stimulating physiological mechanisms to reinforce healing responses without reaching temperatures that can cause permanent tissue damage. The therapeutic outcome is strongly affected by the temperature distribution in the treated region and its accurate monitoring represents an unmet clinical need. In this work, we investigate on the capacities of four-dimensional optoacoustic tomography to monitor tissue heating with MIFU. Calibration experiments in a tissue-mimicking phantom have confirmed that the optoacoustically-estimated temperature variations accurately match the simultaneously acquired thermocouple readings. The performance of the suggested approach in real tissues was further shown with bovine muscle samples. Volumetric temperature maps were rendered in real time, allowing for dynamic monitoring of the ultrasound focal region, estimation of the peak temperature and the size of the heat-affected volume.

1. Introduction

Therapeutic ultrasound (US) comprises a myriad of techniques routinely used in the clinics to treat pathological tissues, such as tumors, kidney stones, neurological disorders, blood clots, hemorrhages or injured muscles and tendons [1,2]. The majority of US-based treatments involve thermal effects produced via tissue heating with average intensity levels exceeding those permitted for diagnostic US imaging purposes ($> 0.1\ W/cm^2$). High-intensity focused ultrasound (HIFU) ($100–10{,}000\ W/cm^2$), is used to selectively destroy abnormal tissues, such as malignant neoplastic lesions, via local temperature elevations exceeding the coagulation thresholds [3,4]. HIFU has been also used at power levels below the thresholds required for ablation, such as in intense therapy ultrasound (ITU), e.g. by creating thermal injury zones in the tissue, initiating tissue repair cascade, promoting collagen generation and thus a healing response [5,6]. Low intensity pulsed ultrasound stimulation (LIPUS) has also shown beneficious effects in tissue healing with typical US intensities lower than $0.1\ W/cm^2$ and a temperature rise less than 1 °C [7]. In addition, non-thermal physical effects, such as cavitation and acoustic streaming, have shown to influence cell membrane permeability and increase cellular activity [8]. Medium-intensity focused ultrasound (MIFU), with acoustic intensity levels between those used in echography and HIFU (typically $5–300\ W/cm^2$), represents a largely unexplored scientific niche that can lead to combined and cooperative thermal and non-thermal physical effects in soft tissues for performing physio or cancer therapy, either directly or via local drug delivery. Dedicated and flexible electronics with programmable parameters – voltage, signal shape, frequency and number of active elements – as well as specialized US array transducers need to be studied and developed to investigate the outcome of US physiotherapy treatments. In our case, using special array transducers and electronics capable to focalize in 3D, temperature increases in phantoms up to 10 °C in less than 30 s have been achieved with intensities of tens of W/cm^2. Tissue heating results from absorption of US waves, while other effects, such as cavitation or acoustic streaming, may additionally take place. Effective application of US requires accurate monitoring of the spatio-temporal temperature distribution during the procedure, control over the delivered US intensity levels and duration of the treatment as well as precise spatial targeting in the body [9].

Considerable inconsistencies in the clinical outcomes for different therapeutic US protocols have been reported [10]. Thereby, the development of efficient monitoring methods is paramount for improving

* Corresponding author.
E-mail address: xl.deanben@helmholtz-muenchen.de (X.L. Deán-Ben).
[1] These authors contributed equally to this work.

https://doi.org/10.1016/j.ultras.2018.11.011
Received 17 May 2018; Received in revised form 1 October 2018; Accepted 26 November 2018
Available online 27 November 2018
0041-624X/

the therapeutic efficacy while avoiding unnecessary tissue damage. Of particular importance is the feasibility to render real-time feedback on the spatio-temporal temperature distribution in the treated tissue. Heat-driven cell deterioration typically starts at temperatures above 50 °C, while cell death strongly depends on the exposure duration to a certain temperature [4]. For instance, coagulative necrosis and immediate cell death is typically produced in HIFU when reaching temperatures above 55 °C for 1 s or longer [11]. Temperature monitoring is also essential in MIFU for preventing overheating. Also, the outcome of a MIFU procedure highly depends on the temperature values and the exposure time. Then, controlling the spatio-temporal distribution of temperature is generally essential in MIFU. Intrusive temperature monitoring methods based on thermocouples, thermistors or fiber-optic detectors can be used for temperature control [12]. However, those are invasive approaches that can only retrieve temperature readings from a limited number of discrete locations. Mapping of the temperature distribution was further attempted using non-invasive imaging approaches, including infrared thermometry [13], analysis of US backscattered signals [14,15], X-ray computed tomography (CT) [16] or magnetic resonance imaging (MRI) [17]. However, all these methods have limitations for real-time volumetric temperature mapping associated to the achievable penetration depth, contrast or spatio-temporal resolution.

Optoacoustic (OA) imaging constitutes an advantageous approach for monitoring thermal treatments as it provides high sensitivity to changes in temperature and can further detect tissue composition changes associated with coagulation [18–21]. OA can reach depths of ~1–2 cm as reported by several groups [22–25], which can be sufficient for many MIFU applications e.g. in physical rehabilitation or pain management [26,27]. To this end, OA monitoring and guidance has been used to control thermal therapies involving radio-frequency ablation [28], laser-induced thermotherapy [29,30], cryoablation [31], therapeutic US procedures including HIFU [32] or nanoparticle-based targeted therapies [33]. One of the advantages of the OA method is the possibility to integrate it with MIFU or HIFU using the same transducer array [34]. Yet, real-time volumetric mapping of the temperature distribution during US thermotherapy, particularly for intensity levels below the thermal damage thresholds, has never been attempted. Herein, using a novel MIFU multi pulse electronic system and a two dimensional piezoelectric spherical matrix array, we demonstrate the feasibility of four dimensional (real-time three-dimensional) optoacoustic mapping of the induced spatio-temporal temperature distribution in a tissue-mimicking phantom and in an ex-vivo bovine tissue sample.

2. Materials and methods

2.1. Experimental set-up and signal processing

A lay-out of the experimental set-up is depicted in Fig. 1a. MIFU heating was induced with a self-developed annular array probe consisting of 8 equal-area coaxial rings, which allowed focusing the US beam along the axial direction. This allows concentrating the energy in a region that resembles an elongated rice grain with approximate dimensions of 1.5–2 mm in width and 1–1.5 cm in length, i.e., the sound beam maximum intensity is confined within a ~0.04 cm^3 volume. The excitation signals in each element were delayed in order to focus the US beam by constructive interference at a distance of 5 cm from the active surface. Each element of the array has an area of 0.88 cm^2 and a central frequency of 2 MHz. The array has a total diameter of 3 cm. The elements were excited with a custom-made multichannel electronic driving system (SITAU, Dasel Sistemas, Madrid, Spain) controlled with a MATLAB® code. When driven with a negative square pulse of 150 V, a peak pressure of 3 MPa is generated at the focus, which corresponds to I_{SPTP} = 300 W/cm^2 of acoustic intensity [5]. The pressure was measured with a needle hydrophone (DAPCO 54389) with 0.6 mm active diameter.

OA volumetric temperature monitoring was performed with a custom-made spherical matrix array consisting of a 256 piezoelectric-elements with 90° (0.59π solid angle) angular coverage [35]. Each element of the array has an area of 3 × 3 mm^2, central frequency of 4 MHz and > 80% detection bandwidth, providing a nearly isotropic imaging resolution of ~200 μm around the geometrical center of the sphere. The OA field of view is in the order of 1 cm^3, which can be covered by the depth of field of the MIFU array. The OA detection array was positioned orthogonally with respect to the MIFU array and acoustic coupling was guaranteed by immersing the entire set-up in water (Fig. 1a). Optoacoustic responses were excited with a short-pulsed (< 10 ns) tunable laser source (Innolas Laser GmbH, Krailling, Germany) guided via a custom-made fiber bundle (CeramOptec GmbH, Bonn, Germany) through a cylindrical cavity in the center of the array. Optical fluence of ~11 mJ cm^{-2} was measured at the surface of the sample at 720 nm illumination wavelength, corresponding to the maximum energy of the laser. The pulse repetition frequency of the laser source was set to 10 Hz. The 256 optoacoustic signals corresponding to all elements of the array were simultaneously acquired at 40 mega-samples per second (MSPS) by a custom-made data acquisition (DAQ) system (Falkenstein Mikrosysteme GmbH, Taufkirchen, Germany) triggered with the Q-switch output of the laser. Synchronization between OA imaging and MIFU excitation was achieved by delaying the US excitation tone-bursts by 100 μs with respect to the laser trigger used for the OA signal acquisition, as depicted in the timing diagram in Fig. 1b. Specifically, the employed MIFU excitation protocol consisted of emitting 50 tone-bursts of 125 (I_{SPTA} = 9.4 W/cm^2) or 255 (I_{SPTA} = 19.1 W/cm^2) cycles with 150 V negative square amplitude and carrier frequency of 2 MHz, at a pulse repetition frequency (PRF) of 1 kHz following each laser pulse. OA images were reconstructed with a graphics processing unit (GPU)-based three-dimensional back-projection algorithm [36]. Prior to reconstruction, the acquired raw signals were deconvolved with the known impulse response of the array elements and band-pass filtered with cut-off frequencies between 0.1 MHz and 6 MHz.

2.2. Temperature estimation method

The OA temperature estimation method is based on the temperature dependence of the Grüneisen parameter, corresponding to the thermoelastic conversion efficiency. For short-pulsed laser excitation under thermal and stress-confinement conditions [37], the optoacoustically-induced pressure amplitude is approximately given by $p_0 = \Gamma \mu_a \Phi$, being Γ the (dimensionless) Grüneisen parameter, μa the optical absorption coefficient and Φ the light fluence. For water and diluted aqueous solutions, the temperature dependence of the Grüneisen parameter can be approximated via [37]

$$\Gamma(T) = 0.0043 + 0.0053T, \quad (1)$$

where T is expressed in °C. Note that Eq. (1) has been previously verified with empirical measurements across a wide range of temperatures [38]. According to Eq. (1), the relative change of the OA signal as a function of temperature increase ΔT can be then expressed as [30]

$$\frac{\Delta p_0}{p_{0,0}} = \frac{0.0053\Delta T}{0.0043 + 0.0053 \cdot T_0} \quad (2)$$

being $p_{0,0}$ and T_0 the initial (baseline) OA signal and the initial temperature, respectively, before the application of MIFU heating. Δp_0 is the increase in OA signal with respect to $p_{0,0}$. According to Eq. (2), the amplitude of the OA signals is expected to increase by approximately 2.7% per degree for temperature levels around 36 °C in living biological tissues. The temperature increment can then be estimated from the relative OA signal increase as

$$\Delta T = \Delta p_0 (0.8113 + T_0)/p_{0,0} \quad (3)$$

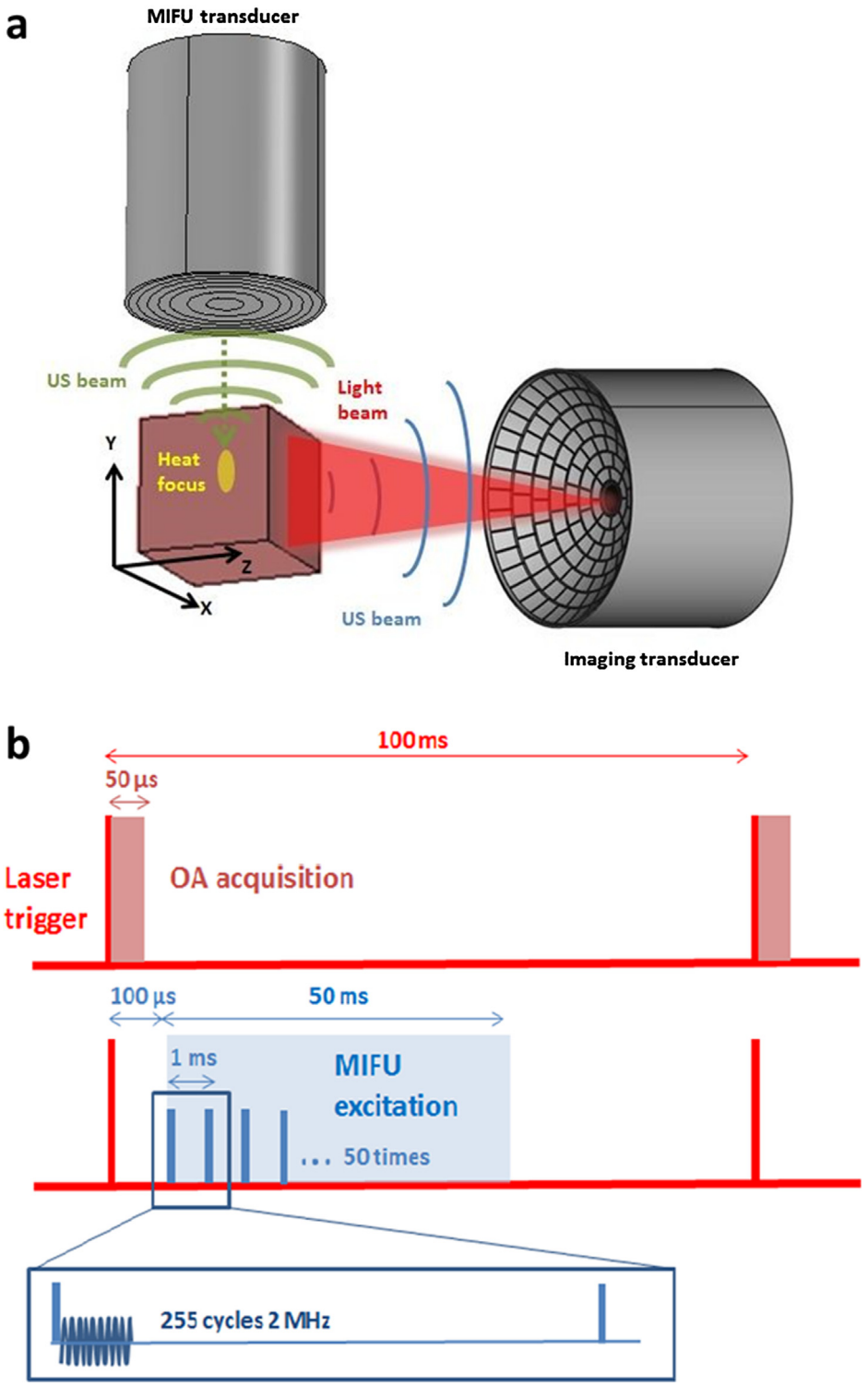

Fig. 1. Lay-out of the experimental setup. (a) Schematic representation of the OA transducer array and the MIFU transducer. (b) Schematic timing diagram of MIFU excitation and OA acquisition.

2.3. Phantom validation experiment

A 8.5 mm wide square-shaped tissue-mimicking phantom was first measured to experimentally test the validity of Eq. (3). The phantom consisted of an agar matrix (1.3% w/w agar powder solved in water) mixed with 7.8% w/w of Aluminum Oxide (Al_2O_3) and India ink to create an US attenuation coefficient of 3.6 $dBcm^{-1}$ at 2 MHz frequency and an optical absorption coefficient of $\mu_a \sim 3.5\,cm^{-1}$ at 720 nm illumination wavelength. The attenuation coefficient was measured using a typical through-transmission approach with two Panametrics A305 2.25 MHz transducers in a water tank. Different samples with various thicknesses were used for comparing the transmitted amplitude. The optical absorption of a water solution with the same concentration of ink and the acoustic attenuation of the phantom material were estimated with an optical spectrometer (OceanOptics, FL, USA) and from the amplitude of multiple echoes of a sample with 1 cm thickness,

respectively. The speed of sound in the phantom material was taken as 1490 m/s, corresponding to the speed of sound in water for the initial temperature. A thermocouple (Physitemp Instruments Inc., Clifton, New Jersey) was inserted at the front (illuminated) edge of the phantom. The temperature readings were digitized with an integrated NI 9213 DAQ (National Instruments Corporation, Austin, Texas, U.S.). The OA-based temperature estimation method, as described in Eqs. (1)–(3), was used to estimate the temperature at a region of interest (ROI) matching the known location of the thermocouple. This corresponds to the region for which a maximum relative increase in the OA signal was measured. Likewise, the US focus was positioned on the thermocouple tip by raster-scanning the MIFU array until the maximum temperature elevation was measured.

2.4. Ex-vivo bovine tissue experiments

The effectiveness of the proposed approach for temperature mapping in real tissues was subsequently examined in an ex-vivo bovine sample. In a first step, the capability to localize the US focus in a three-dimensional region was tested. For this, the MIFU array was scanned along the axial direction of the OA imaging probe. For each position, the MIFU array was driven as previously described. Considering that no significant thermal diffusion occurs for the protocol duration (15 s), the temperature raise within this time period is assumed to be mainly due to US absorption and so the focus position can be localized. In addition, the spatio-temporal distribution of temperature was estimated during MIFU heating for a fixed position of the US focus. The baseline tissue temperature was $T_0 = 22\,^{\circ}C$. MIFU heating was stopped after 15 s while the OA monitoring continued for 40 s to cover the cooling period. The expected optical absorption coefficient in this type of tissue is approximately $0.2\,cm^{-1}$ [39]. The ultrasound attenuation at 2 MHz was estimated as that of muscle tissue ($1.09\,dB\,cm^{-1}$) [40]. This is in agreement with lower temperature increase observed as compared to that of the phantom.

3. Results

3.1. Phantom validation experiment

Fig. 2a shows a schematic representation of the measurement arrangement. The maximum intensity projection (MIP) along the depth direction of the volumetric OA images taken before the MIFU heating is displayed in Fig. 2b. The temperature increase in the phantom at the thermocouple location was then estimated with Eq. (3). Specifically, two measurements were performed. First, a series of 150 V tone-bursts consisting of 255 cycles (I_{SPTA} = 19.1 W/cm^2) were used to excite the MIFU array for 15 s. In Fig. 2c, the time dependence of temperature measured with the thermocouple versus the temperature estimated from the OA image sequence are represented by the solid and dashed blue lines, respectively. In a second measurement, a series of tone-bursts of 150 V and 125 cycles (I_{SPTA} = 9.4 W/cm^2) were used to drive the MIFU array for 20 s. The corresponding temperature values are shown by solid and dashed red lines in Fig. 2c. The relative OA signal increases were estimated with a reference OA image (the baseline signal) taken as the average of 30 frames immediately preceding the MIFU procedure. It is shown that the optoacoustically-estimated temperature acceptably matches the thermocouple readings. Specifically, the standard deviations of the differences between the corresponding time profiles in Fig. 2c are 0.65 °C and 0.88 °C for tone-bursts of 125 and 255 cycles, respectively. The good agreement is probably a consequence of the fact that the phantom consists of an aqueous solution, for which Eq. (3) is expected to be valid [30]. Inaccuracies may originate from the discrepancy between the actual location of the thermocouple tip and the analyzed OA traces.

3.2. Ultrasonic focus monitoring

The difference of the OA images of the bovine tissue taken after and before MIFU heating (150 V tone-bursts, 255 cycles, I_{SPTA} = 19.1 W/cm^2) are displayed in Fig. 3. The tissue surface is indicated with a dashed line. No significant heat diffusion was produced during the heating period, so that the differential images reliably represent the heated region, namely, the US focus. The difference in the signal amplitude for the different US focus depths is due to light attenuation, which also

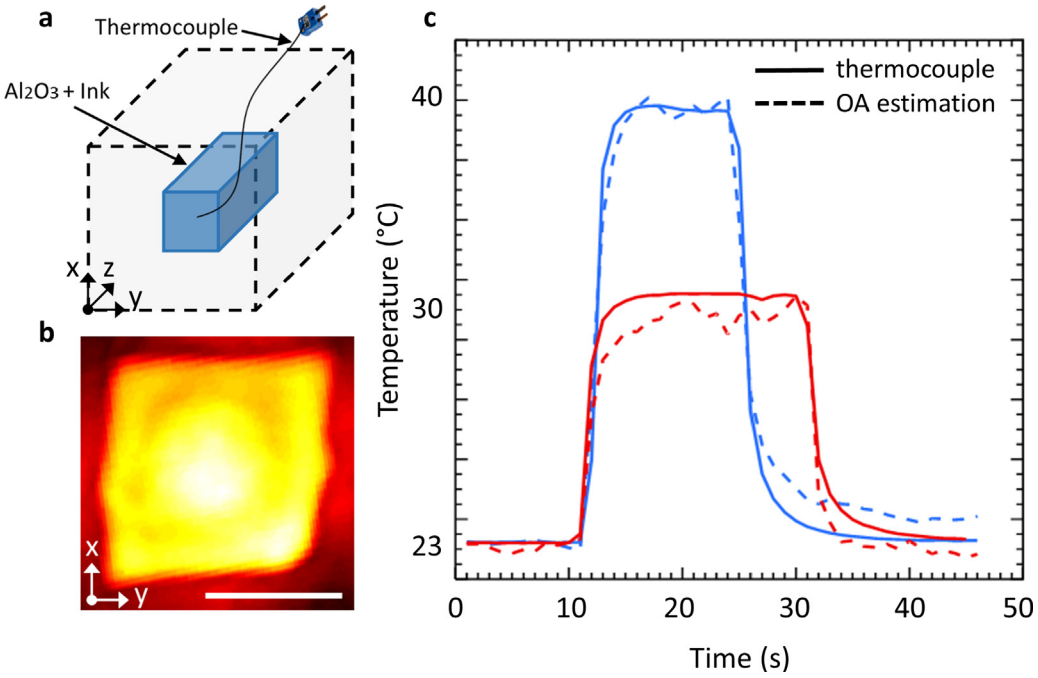

Fig. 2. Validation of the OA temperature monitoring method. (a) Thermocouple location in the tissue mimicking phantom. (b) MIP of the 3D OA image along the z direction, showing the front side of the phantom. Scalebar – 5 mm. (c) OA temperature estimations (dashed lines) along with the corresponding thermocouple readings (continuous lines). The data corresponds to two different MIFU heating procedures using 255 (blue) and 125 (red) cycles. (For interpretation of the references to color in this figure legend, the reader is referred to the web version of this article.)

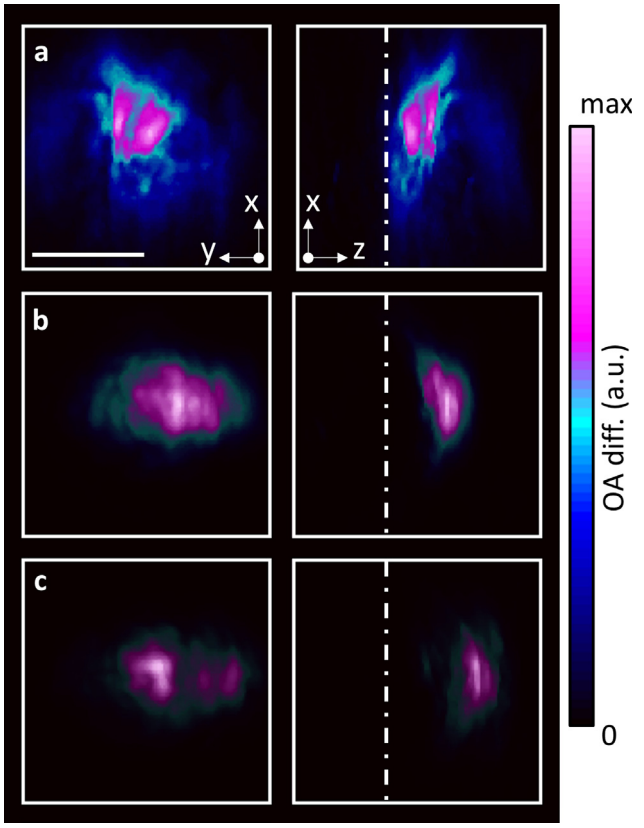

Fig. 3. MIPs of the differential 3D OA images along the z and y directions from ex-vivo bovine tissue for the US focus located at a reference position right underneath the tissue surface (a) and at 1.5 mm (b) and 3 mm (c) points deeper than the reference position, respectively. Scalebar – 5 mm.

results in a lower signal to noise ratio (SNR) at deeper locations. This in turn limits the maximum applicable depth for OA monitoring of the MIFU treatments.

3.3. Temperature mapping in ex-vivo bovine tissue

The results of the temperature mapping experiment in an *ex-vivo* bovine tissue sample are shown in Fig. 4. Specifically, the spatio-temporal maps of the temperature elevation estimated according to Eq. (3) are displayed in Fig. 4a. Note that no thermocouple was included in this case. Indeed, it was found that it generates a significantly larger optoacoustic signal than the tissue. This leads to streak-type artefacts in the reconstructed images that also affect the estimated temperature maps. It can be seen that the temperature map estimated for the time point of peak temperature elevation (Fig. 4a, 20 s) is tightly centered around the ultrasonic focus location. On the other hand, the heated region spreads over a larger region at later time points during the cooling period (Fig. 4a, 24 s), which indicates that thermal diffusion plays a dominant role in carrying the heat further away from the ultrasonic focus. This is further corroborated in the time traces in Fig. 4b, corresponding to the estimated temperatures at three locations indicated in Fig. 4a at 2.5 s. The incremental heating and thermal diffusion processes can be best identified in a video displaying real-time volumetric monitoring of the temperature map distribution in bovine tissue (Visualization 1). It can be appreciated that voxels closer to the ultrasonic focus experience greater temperature increases and reach the maximum value when the MIFU transducer is turned off. Yet, the generated heat continues diffusing outside the focal region also at later time points. Since the estimated temperature rise was below 15 °C during the entire procedure, no tissue damage should be produced. This was confirmed by visual inspection of the sample after the experiment.

4. Discussion and conclusion

Medium-intensity focused ultrasound (MIFU) therapy aims to provide significant improvements in the efficacy, safety, reliability and metrological traceability of US treatments in both physiotherapy and drug delivery. Here, four-dimensional OA tomography was used to non-invasive measure the temperature increase induced in tissues by a newly designed MIFU prototype system. Of particular importance is the feasibility to provide real-time volumetric temperature feed-back, which can greatly impact the outcome of MIFU-based medical treatments by (1) enabling effective control of the exposure time of the target tissue at a given temperature and (2) preventing tissue overheating above the damage threshold. OA is particularly suitable for temperature mapping applications due to the high sensitivity of the Grüneisen parameter, representing the OA conversion efficiency, to temperature variations [37,41]. Note that in our current experiments the temperature distribution was estimated by assuming the Grüneisen parameter to be equivalent to that of water. Considering that muscle tissues contain approximately 75% water, 20% protein, 1–10% fat and 1% glycogen, this seems a reasonable approximation [42]. However, accurate calibration of the temperature dependence of the Grüneisen parameter is required to assess the error in such approximation and to improve the accuracy of the estimated temperature values. Such calibration may be achieved with optoacoustic methods, for which the light fluence and the absorption coefficient of the tissue of interest need to be determined [43]. This turns particularly challenging *in vivo*, while the optical properties *ex vivo* can significantly change. The high spatio-temporal resolution of the state-of-the-art OA tomography system employed further represents an important advantage. In this work, we have attained spatial resolution of 200 μm at 10 Hz volumetric frame rates, which covers well the spatio-temporal range of the induced temperature variations. Higher spatial and temporal resolutions are also possible by using a similar configuration, which however would come to the detriment of the field of view [44].

It has further been shown that four-dimensional OA tomography enables dynamic localization of the position of the US focus. In this way, more accurate identification of the target tissues can be facilitated prior to applying the therapy. Naturally, the SNR of the differential OA images declines with depth due to light attenuation, the latter dominating over acoustic attenuation for the applicable US frequency range [45]. In order to improve on the achievable monitoring depth, other light delivery methods, e.g. based on endoscopic or intravascular probes, may be additionally considered [46,47]. The regions accessible with OA imaging are confined within ~1–2 cm from the surface where light is delivered. This is sufficient for many relevant potential applications of MIFU, such as treatment of active myofascial pain trigger points, stimulation of abdominal or paraspinal muscles or even for neurostimulation of cortical areas in the brain. Registration of OA and US images can further provide enhanced anatomical information and some efficient techniques for hybrid optoacoustic-ultrasound (OPUS) imaging have been recently reported [48].

The monitoring approach introduced in this work can also be potentially applied in treatments based on selective tissue destruction with HIFU [49,50]. These procedures can particularly benefit from augmented information acquired by means of multispectral optoacoustic tomography (MSOT) analysis [51]. The most recently developed OA systems effectively provide five-dimensional (real-time three-dimensional multispectral) imaging capabilities [52], thus enabling tracking of spectroscopic variations in the target tissue, e.g. due to coagulation. It should be noted that the temperature dependence of the OA signals in biological tissues is significantly altered at temperatures exceeding 50 °C [19], so that more accurate calibration are needed for temperature monitoring in coagulated tissue volumes. The temperature maps in vivo are also expected to be affected by induced changes in blood flow, which have a cooling effect. The development of proper models accounting for different effects occurring in living organisms

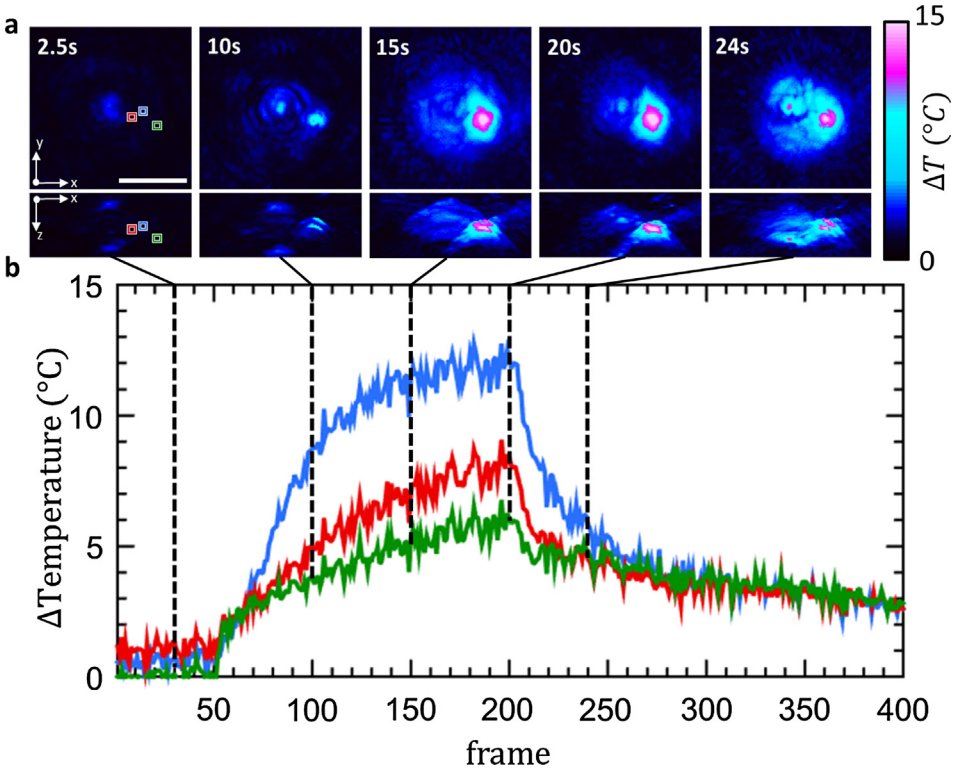

Fig. 4. Volumetric OA monitoring of temperature during MIFU therapy performed in an ex-vivo bovine tissue. (a) MIPs of the estimated 3D temperature increase maps at different time points along the procedure. Scalebar – 5 mm. (b) Temporal profiles of the estimated temperature increase for the 3 points labeled in (a) with the same color. (For interpretation of the references to color in this figure legend, the reader is referred to the web version of this article.)

thus represent an important next step. Also, a temperature rise induces changes in the speed of sound of the heat affected zone, which may affect the reconstructed images obtained by assuming a uniform speed of sound [53], particularly if high-resolution is required.

In conclusion, it has been shown that tissue heating with US can be monitored in three dimensions and in real time with OA tomography. The achieved high sensitivity to temperature variations, high spatial resolution and fast imaging rates anticipate applicability of the suggested approach in various procedures involving low and medium intensity therapeutic US, such as physical rehabilitation [26,54,55], pain management [27] or neurostimulation [56].

Acknowledgements

The authors acknowledge support from the German Research Foundation (DFG) under Research Grant RA 1848/5-1 (D.R.) and the Spanish Ministry of Economy and Competitiveness under project DPI2016-80254-R (F.M.).

Appendix A. Supplementary material

Supplementary data to this article can be found online at https://doi.org/10.1016/j.ultras.2018.11.011.

References

[1] G. ter Haar, Heat and sound: focused ultrasound in the clinic, Int. J. Hyperth. 31 (2015) 223–224.
[2] E.S. Ebbini, G. Ter Haar, Ultrasound-guided therapeutic focused ultrasound: current status and future directions, Int. J. Hyperth. 31 (2015) 77–89.
[3] Y.-S. Kim, H. Rhim, M.J. Choi, H.K. Lim, D. Choi, High-intensity focused ultrasound therapy: an overview for radiologists, Korean J. Radiol. 9 (2008) 291–302.
[4] K.F. Chu, D.E. Dupuy, Thermal ablation of tumours: biological mechanisms and advances in therapy, Nat. Rev. Cancer 14 (2014) 199–208.
[5] T.D. Mast, et al., Bulk ablation of soft tissue with intense ultrasound: modeling and experiments, J. Acoust. Soc. Am. 118 (2005) 2715–2724.
[6] M.H. Slayton, J.K. Barton, Ultrasonics Symposium (IUS), 2014 IEEE International, IEEE, 2014, pp. 1654–1657.
[7] A. Khanna, R.T. Nelmes, N. Gougoulias, N. Maffulli, J. Gray, The effects of LIPUS on soft-tissue healing: a review of literature, Brit. Med. Bull. 89 (2008) 169–182.
[8] D.M. Hallow, A.D. Mahajan, T.E. McCutchen, M.R. Prausnitz, Measurement and correlation of acoustic cavitation with cellular bioeffects, Ultrasound Med. Biol. 32 (2006) 1111–1122.
[9] G. Clement, Perspectives in clinical uses of high-intensity focused ultrasound, Ultrasonics 42 (2004) 1087–1093.
[10] D.L. Miller, et al., Overview of therapeutic ultrasound applications and safety considerations, J. Ultrasound Med. 31 (2012) 623–634.
[11] G. ter Haar, C. Coussios, High intensity focused ultrasound: physical principles and devices, Int. J. Hyperth. 23 (2007) 89–104.
[12] E. Schena, D. Tosi, P. Saccomandi, E. Lewis, T. Kim, Fiber optic sensors for temperature monitoring during thermal treatments: an overview, Sensors-Basel 16 (2016) 1144.
[13] B. Lahiri, S. Bagavathiappan, T. Jayakumar, J. Philip, Medical applications of infrared thermography: a review, Infrared Phys. Techn. 55 (2012) 221–235.
[14] T.A. Fuhrmann, O. Georg, J. Haller, K.-V. Jenderka, V. Wilkens, Uncertainty estimation for temperature measurement with diagnostic ultrasound, J. Ther. Ultrasound 4 (2016) 28.
[15] M.A. Lewis, R.M. Staruch, R. Chopra, Thermometry and ablation monitoring with ultrasound, Int. J. Hyperth. 31 (2015) 163–181.
[16] F. Fani, E. Schena, P. Saccomandi, S. Silvestri, CT-based thermometry: an overview, Int. J. Hyperth. 30 (2014) 219–227.
[17] V. Rieke, K. Butts Pauly, MR thermometry, J. Magn. Reson. Imaging 27 (2008) 376–390.
[18] K.V. Larin, I.V. Larina, M. Motamedi, R.O. Esenaliev, Biomedical Optoacoustics, International Society for Optics and Photonics, 2000, pp. 311–322.
[19] K.V. Larin, I.V. Larina, R.O. Esenaliev, Monitoring of tissue coagulation during thermotherapy using optoacoustic technique, J. Phys. D Appl. Phys. 38 (2005) 2645.
[20] J. Kandulla, H. Elsner, R. Birngruber, R. Brinkmann, Noninvasive optoacoustic online retinal temperature determination during continuous-wave laser irradiation, J. Biomed. Opt. 11 (2006) 041111-041111-041113.
[21] E. Petrova, et al., Using optoacoustic imaging for measuring the temperature dependence of Grüneisen parameter in optically absorbing solutions, Opt. Express 21 (2013) 25077–25090.
[22] L.V. Wang, Multiscale photoacoustic microscopy and computed tomography, Nat. Photon. 3 (2009) 503.
[23] I. Stoffels, et al., Metastatic status of sentinel lymph nodes in melanoma determined noninvasively with multispectral optoacoustic imaging, Sci. Transl. Med. 7 (2015) 317ra199–317ra199.
[24] X.L. Deán-Ben, T.F. Fehm, M. Gostic, D. Razansky, Volumetric hand-held optoacoustic angiography as a tool for real-time screening of dense breast, J. Biophoton. 9 (2016) 253–259.
[25] M. Heijblom, et al., Photoacoustic image patterns of breast carcinoma and comparisons with Magnetic Resonance Imaging and vascular stained histopathology, Sci. Rep.-UK 5 (2015) 11778.
[26] L. Claes, B. Willie, The enhancement of bone regeneration by ultrasound, Prog. Biophys. Mol. Biol. 93 (2007) 384–398.
[27] J. Majlesi, H. Ünalan, High-power pain threshold ultrasound technique in the

treatment of active myofascial trigger points: a randomized, double-blind, case-control study, Arch. Phys. Med. Rehabil. 85 (2004) 833–836.
[28] G.A. Pang, E. Bay, X. Deán-ben, D. Razansky, Three-dimensional optoacoustic monitoring of lesion formation in real time during radiofrequency catheter ablation, J. Cardiovasc. Electr. 26 (2015) 339–345.
[29] T.F. Fehm, X.L. Deán-Ben, P. Schaur, R. Sroka, D. Razansky, Volumetric optoacoustic imaging feedback during endovenous laser therapy–an ex vivo investigation, J. Biophoton. 9 (2016) 934–941.
[30] F.J.O. Landa, X.L. Deán-Ben, R. Sroka, D. Razansky, Volumetric optoacoustic temperature mapping in photothermal therapy, Sci. Rep.-UK 7 (2017) 9695.
[31] E.V. Petrova, M. Motamedi, A.A. Oraevsky, S.A. Ermilov, in: Proc. SPIE. 97080G.
[32] P.V. Chitnis, H.-P. Brecht, R. Su, A.A. Oraevsky, Feasibility of optoacoustic visualization of high-intensity focused ultrasound-induced thermal lesions in live tissue, J. Biomed. Opt. 15 (2010) 021313-021313-021315.
[33] Y. Lyu, et al., Intraparticle molecular orbital engineering of semiconducting polymer nanoparticles as amplified theranostics for in vivo photoacoustic imaging and photothermal therapy, Acs Nano 10 (2016) 4472–4481.
[34] A. Prost, A. Funke, M. Tanter, J.-F. Aubry, E. Bossy, Photoacoustic-guided ultrasound therapy with a dual-mode ultrasound array, J. Biomed. Opt. 17 (2012) 0612051–0612056.
[35] X.L. Dean-Ben, D. Razansky, Portable spherical array probe for volumetric real-time optoacoustic imaging at centimeter-scale depths, Opt. Express 21 (2013) 28062–28071, https://doi.org/10.1364/Oe.21.028062.
[36] X.L. Dean-Ben, A. Ozbek, D. Razansky, Volumetric real-time tracking of peripheral human vasculature with GPU-accelerated three-dimensional optoacoustic tomography, IEEE Trans. Med. Imaging 32 (2013) 2050–2055.
[37] L.V. Wang, H.-I. Wu, Biomedical Optics: Principles and Imaging, John Wiley & Sons, 2012.
[38] W. Wang, A. Mandelis, Thermally enhanced signal strength and SNR improvement of photoacoustic radar module, Biomed. Opt. Express 5 (2014) 2785–2790.
[39] S.L. Jacques, Optical properties of biological tissues: a review, Phys. Med. Biol. 58 (2013) R37.
[40] M.O. Culjat, D. Goldenberg, P. Tewari, R.S. Singh, A review of tissue substitutes for ultrasound imaging, Ultrasound Med. Biol. 36 (2010) 861–873, https://doi.org/10.1016/j.ultrasmedbio.2010.02.012.
[41] M. Pramanik, L.V. Wang, Thermoacoustic and photoacoustic sensing of temperature, J. Biomed. Opt. 14 (2009) 054024.
[42] A. Listrat, et al., How muscle structure and composition influence meat and flesh quality, Sci. World J. 2016 (2016).
[43] D.-K. Yao, C. Zhang, K.I. Maslov, L.V. Wang, Photoacoustic measurement of the Grüneisen parameter of tissue, J. Biomed. Opt. 19 (2014) 017007.
[44] X.L. Deán-Ben, et al., Functional optoacoustic neuro-tomography for scalable whole-brain monitoring of calcium indicators, Light Sci. Appl. 5 (2016) e16201.
[45] X.L. Dean-Ben, D. Razansky, V. Ntziachristos, The effects of acoustic attenuation in optoacoustic signals, Phys. Med. Biol. 56 (2011) 6129–6148, https://doi.org/10.1088/0031-9155/56/18/021.
[46] H. He, A. Buehler, V. Ntziachristos, Optoacoustic endoscopy with curved scanning, Opt. Lett. 40 (2015) 4667–4670.
[47] A. Rosenthal, et al., Sensitive interferometric detection of ultrasound for minimally invasive clinical imaging applications, Laser Photon. Rev. 8 (2014) 450–457.
[48] X. Deán-Ben, E. Merčep, D. Razansky, Hybrid-array-based optoacoustic and ultrasound (OPUS) imaging of biological tissues, Appl. Phys. Lett. 110 (2017) 203703.
[49] H. Cui, X. Yang, Real-time monitoring of high-intensity focused ultrasound ablations with photoacoustic technique: an in vitro study, Med. Phys. 38 (2011) 5345–5350.
[50] J. Gray, et al., Multi-wavelength photoacoustic visualization of high intensity focused ultrasound lesions, Ultrason. Imaging 38 (2016) 96–112.
[51] S. Tzoumas, N. Deliolanis, S. Morscher, V. Ntziachristos, Unmixing molecular agents from absorbing tissue in multispectral optoacoustic tomography, IEEE Trans. Med. Imaging 33 (2014) 48–60.
[52] X.L. Deán-Ben, D. Razansky, Adding fifth dimension to optoacoustic imaging: volumetric time-resolved spectrally enriched tomography, Light Sci. Appl. 3 (2014) e137.
[53] J. Yao, H. Ke, S. Tai, Y. Zhou, L.V. Wang, Absolute photoacoustic thermometry in deep tissue, Opt. Lett. 38 (2013) 5228–5231.
[54] G. Ter Haar, Therapeutic ultrasound, Eur. J. Ultrasound 9 (1999) 3–9.
[55] V.J. Robertson, K.G. Baker, A review of therapeutic ultrasound: effectiveness studies, Phys. Ther. 81 (2001) 1339–1350.
[56] R.L. King, J.R. Brown, W.T. Newsome, K.B. Pauly, Effective parameters for ultrasound-induced in vivo neurostimulation, Ultrasound Med. Biol. 39 (2013) 312–331.